

Article

Modelling and Simulation of Heat Exchanger with Strong Dependence of Oil Viscosity on Temperature

Dinara Kurmanova ¹, Nurbolat Jaichibekov ¹ , Anton Karpenko ² and Konstantin Volkov ^{3,*}¹ Faculty of Mechanics and Mathematics, Eurasian National University, Astana 010008, Kazakhstan² Faculty of Mathematics and Mechanics, St. Petersburg State University, 198504 St. Petersburg, Russia³ Faculty of Science, Engineering and Computing, Kingston University, London SW15 3DW, UK

* Correspondence: k.volkov@kingston.ac.uk

Abstract: The heating of oil and oil products is widely used to reduce energy losses during transportation. An approach is developed to determine the effective length of the heat exchanger and the temperature of the cold coolant (oil) at its outlet in the case of a strong dependence of oil viscosity on temperature. Oil from the Uzen field (Kazakhstan) is considered as a heated coolant, and water is considered as a heating component. The method of the log–mean temperature difference, modified for the case of variable viscosity, and the methods of computational fluid dynamics (CFD) are used for calculations. The results of the numerical calculations are compared with the data obtained on the basis of a theoretical approach at a constant viscosity. When using a theoretical approach with a constant or variable viscosity, the heat transfer coefficients to cold and hot coolants are found using criterion dependencies. The Reynolds-averaged Navier–Stokes (RANS) and a turbulence model that takes into account the laminar–turbulent transition are applied. In the case of variable oil viscosity, a transition from the laminar flow regime to the turbulent one is manifested, which has a significant effect on the effective length of the heat exchanger. The obtained results of the CFD calculations are of interest for the design of heat exchangers of a new type, for example, helicoid ones.

Keywords: energy; heat transfer; viscosity; fluid dynamic; oil; numerical simulation; laminar–turbulent transition

**Citation:** Kurmanova, D.;

Jaichibekov, N.; Karpenko, A.; Volkov, K. Modelling and Simulation of Heat Exchanger with Strong Dependence of Oil Viscosity on Temperature.

Fluids **2023**, *8*, 95. <https://doi.org/10.3390/fluids8030095>

Academic Editors: Lioua Kolsi and Mehrdad Massoudi

Received: 1 February 2023

Revised: 1 March 2023

Accepted: 6 March 2023

Published: 8 March 2023



Copyright: © 2023 by the authors. Licensee MDPI, Basel, Switzerland. This article is an open access article distributed under the terms and conditions of the Creative Commons Attribution (CC BY) license (<https://creativecommons.org/licenses/by/4.0/>).

1. Introduction

The change in the qualitative state of the raw material base leads to development and involvement in the operation of oil fields with high contents of paraffins, resins, and asphaltenes. The development of such deposits requires the use of unconventional methods of oil production and its preparation for transportation. Light oil products (gasoline, kerosene, etc.) are easily transported through pipelines at any time of the year and operations with them do not cause any particular difficulties. The operations with dark oil products (fuel oil, lubricating oils, etc.) and crude oil cause significant difficulties due to the fact that dark oil products become more viscous when the air temperature drops, and their transportation without heating becomes impossible. For the pipeline transportation of oil and oil products, an approach is used based on the regulation of the rheological properties of oil, for example, by heating the oil with its subsequent transportation through a pipeline with increased thermal insulation (hot oil transfer). In some cases, an increase in the viscosity of oil with a decrease in temperature leads to unacceptable stresses on the walls of the pipeline and stops transportation.

Heat exchange processes are carried out in heat exchangers of various types and designs [1–5]. For heating, various heat carriers are used, for example, hot water or steam. Energy consumption is one of the important factors that has a significant impact on the choice of heat exchanger design [6]. In the oil and gas industry, shell and tube heat exchangers are used, which provide good performance characteristics over a wide range of operating conditions, high reliability, and low cost. To determine the efficiency of

heat exchange processes, final temperatures and the required operating parameters of heat carriers, a thermal calculation is performed.

The composition of oil (in particular, the content of asphaltenes, resins, and paraffins) has a significant effect on the dependence of viscosity on temperature [7,8]. Empirical formulas describing the change in kinematic viscosity depending on temperature have the form of various functions (exponential, polynomial, power, etc.), which are characterized by the presence of coefficients that depend on the properties of the liquid. Constant coefficients are determined based on measurements of kinematic viscosity at several points. To calculate the thermodynamic parameters of oil, gas condensates, and their fractions, the generalized Lee–Kessler equation of state [9] is used. The dependence of the kinematic viscosity of oil and oil mixtures on temperature is analysed in [10], where the existing formulas for calculating the kinematic viscosity of oil in main pipelines are compared.

The fluid flow in the annular space of the heat exchanger is complex and depends on many factors. The numerical modelling of heat transfer in heat exchange devices of various designs is carried out in [11,12]. The results of the numerical calculations are used to find the optimal ways to intensify heat transfer processes [13–15]. The results obtained indicate a decrease in the effect of the viscosity of the pumped oil on the hydraulic characteristics of the pipeline when pumping in developed turbulent regimes.

A comparison of the accuracy of various turbulence models used to close the Reynolds-averaged Navier–Stokes (RANS) equations is the subject of study in [16–19]. Two-parameter turbulence models, including the k – ε model, k – ω model, and SST model, are used in the CFD calculations. The obtained results are in satisfactory agreement with the data of the industrial experiments. This allows for solving the problems of process control and increasing production efficiency and determining the optimal regime parameters of technological processes. At the same time, the available calculations using two-parameter turbulence models do not take into account the laminar–turbulent transition, which affects the determination of the effective length of the heat exchanger.

Many experimental and computational works have been performed before, and various flow arrangements and methods of enhancement of heat transfer have been proposed and investigated [20–23]. In classical heat exchangers, a tube bundle for one coolant is placed inside a casing along which another coolant moves. In the design of helicoid heat exchangers, profiled tubes and screw profile fins are used, with the help of which heat exchange conditions are improved. The tubes have a small diameter and thin walls (about 0.3 mm). In the case where the viscosity depends on temperature, the flow regime in such thin tubes changes from laminar to turbulent.

Reducing the viscosity of oil by heating it is one of the ways to increase the energy efficiency of the process of pumping high-viscosity oil during production and transportation. Performing numerical simulation allows for solving a number of issues related to improving the efficiency of heat transfer, which remains one of the most important in the design of heat exchange devices in the oil and gas industry. The laminar–turbulent transition plays a significant role in a new type of heat exchangers, for example, helicoid ones, consisting of a large number of long thin profiled tubes and being characterized by a high speed of the heat carriers used. In this study, a mathematical model of a heat exchanger is developed that takes into account the laminar–turbulent transition. For simplicity, a “pipe in pipe” heat exchanger scheme with a thin and smooth inner tube is selected. A calculation method is provided for a parallel flow heat exchanger, in which the working fluid in the inner pipeline is oil (cold coolant), and, in the outer pipe, it is water (hot coolant). The calculations are carried out for a model design of a heat exchanger both using a theoretical approach based on the Log–Mean Temperature Difference (LMTD) method at constant and variable viscosity, and based on Computational Fluid Dynamics (CFD) tools. The data obtained within the framework of various approaches are compared with each other, which causes it to be possible to draw a conclusion about the accuracy of each of the approaches and the possibility of their application in practice.

2. Dependence of Viscosity on Temperature

The Uzen oil and gas field is located in the Mangistau region of Kazakhstan. The oil deposits are deep 0.9–2.4 km. The oil density is 844–874 kg/m³, dynamic viscosity is 3.4–8.15 mPa·c, content of sulphur is 0.16–2%, content of paraffins is 16–22%, and content of resins is 8–20%.

In the literature, various formulas are used to take into account the dependence of viscosity on temperature. In the oil industry, temperature-dependent kinematic viscosity, the Walther formula is widely used [10]:

$$\lg[\lg(\nu + 0.8)] = a + b \lg T, \quad (1)$$

where a and b are empirical coefficients experimentally determined. The coefficients a and b in the Formula (1) are found from the relations

$$a = \lg[\lg(\nu_1 + 0.8)] - b \lg T_1;$$

$$b = \frac{\lg[\lg(\nu_1 + 0.8)] - \lg[\lg(\nu_2 + 0.8)]}{\lg T_1 - \lg T_2}.$$

Here, ν_1 and ν_2 are kinematic viscosity values at temperatures T_1 and T_2 .

The comparison of the results of calculations using the Voltaire formula with the experimental values of dynamic viscosity is shown in Figure 1 for oil from the Uzen field. The solid line corresponds to the dependence of the viscosity on temperature, obtained using the Walther Formula (1), and the triangular icons correspond to the results of a physical experiment [24].

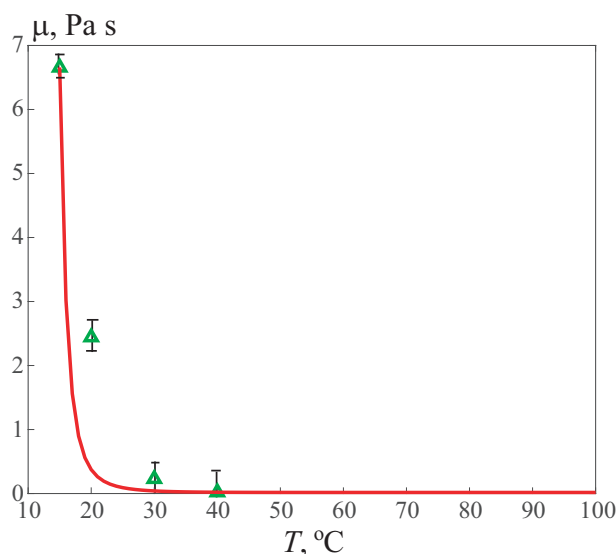


Figure 1. The dependence of the dynamic viscosity of oil from the Uzen field on temperature. Triangular symbols correspond to the experimental data [24], and solid line correspond to the calculations using the Walther formula.

The rheological properties of oil are considered as a property of a colloidal and dispersed system, which, under certain conditions, is prone to the formation of bulk structures with pronounced thixotropy. The rheological parameters of oil are experimentally estimated by the nature of the dependence of shear stresses on the shear gradient.

In a state of equilibrium, the oil system behaves similar to a plastic fluid and has some spatial structures that can resist shear stress until its value exceeds the value of the static shear stress. After reaching a certain shear rate, the oil is able to flow as a Newtonian fluid. An example of a plastic fluid are oils with a high paraffin content at temperatures below

the crystallization temperature, abnormally viscous oils, with a high content of asphaltenes, and structured colloidal systems used for enhanced oil recovery.

The viscosity of Newtonian oil does not depend on the deformation mode and is constant. Such oil is characterized by a relatively low content of resins, mainly not exceeding 15–20%. The oils with a low content of high-melting paraffins, as a rule, do not form structures and are classified as Newtonian liquids. For non-Newtonian oil, the viscosity during movement changes with time, since the destruction of the spatial structure is constantly occurring. The structural and mechanical properties of non-Newtonian oil disappear when heated.

The properties of oil from the Uzen field allow it to be attributed to Newtonian fluids. The Newtonian model can be used as a basis for research. This is all the more true for the use of various turbulence models, which, as a rule, are tested on a number of problems for media exhibiting Newtonian properties.

3. Method for Constant Viscosity

To estimate heat flux from a hot coolant to a cold coolant, a model of a coolant with a constant viscosity along the length is used, based on the use of the log-mean temperature difference. In a recuperative heat exchanger, two fluids with different temperatures move in a space separated by a solid wall (Figure 2). The thermal calculation is reduced to the coupled solution of the equations of the heat balance and heat transfer.

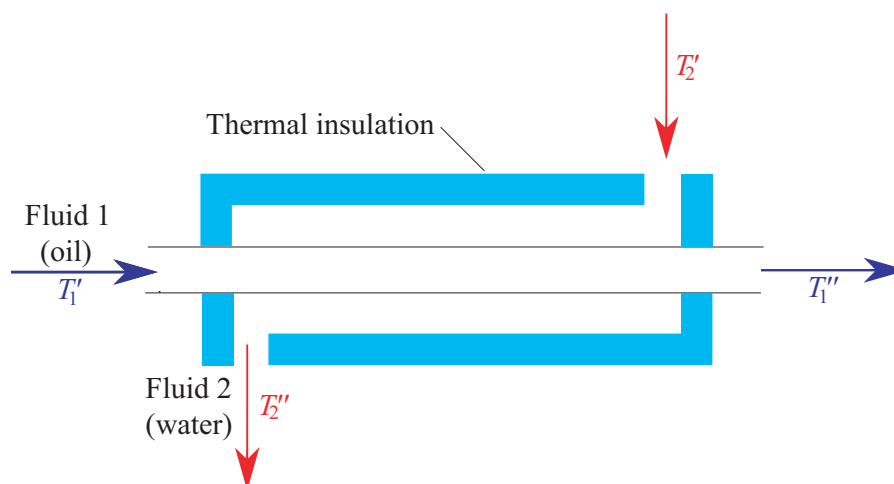


Figure 2. Scheme of counterflow heat exchanger.

The energy balance equation has the form [25]:

$$Q = G_1 c_{p1} (T_1' - T_1'') = G_2 c_{p2} (T_2'' - T_2') > 0. \tag{2}$$

Here, Q is amount of heat transferring from hot stream to cold stream, G is the mass flow rate, c_p is the specific heat capacity, T' is the inlet temperature, and T'' is the outlet temperature. Subscript 1 corresponds to the hot stream, and subscript 2 corresponds to the cold stream.

The heat transfer equation for a heat exchanger is represented as

$$Q = \bar{k} F \Delta \bar{T}, \tag{3}$$

where \bar{k} is the average heat transfer coefficient calculated at average temperature $(T_1' + T_1'')/2$ and $(T_2' + T_2'')/2$, $\Delta \bar{T}$ is the average temperature difference. The average temperature difference is defined as

$$\Delta\bar{T} = \frac{1}{F} \int_0^F \Delta T dF,$$

where F is the surface area.

Defining $\Delta T = (T_1 - T_2)$, Equations (2) and (3) are written in differential form:

$$\frac{d(\Delta T)}{\Delta T} = -mk dF, \quad m = \left(\frac{1}{G_1 c_{p1}} \pm \frac{1}{G_2 c_{p2}} \right).$$

The plus sign is chosen in the case of a parallel heat exchanger, and the minus sign is chosen in the case of a counterflow heat exchanger. The equation is valid along the direction of movement of the hot stream. Assuming that m and \bar{k} are constant over the length, integration from 0 to F and from $\Delta T'$ and ΔT leads to the equation

$$\Delta T = \Delta T' \exp(-m\bar{k}F), \tag{4}$$

where $\Delta T'$ is temperature difference at the inlet of the hot coolant. The temperature difference along the heat exchange surface changes exponentially. By averaging the temperature difference over the entire heat exchange surface, the logarithmic mean temperature difference is found from the relation

$$\bar{\Delta T} = \frac{\Delta T'' - \Delta T'}{\ln(\Delta T''/\Delta T')}.$$

In the design calculation of heat exchanges, the amount of heat Q is determined using Equation (2). The area of the heat exchange surface F is found from the equation

$$F = \frac{Q}{\bar{k} \bar{\Delta T}}.$$

When calculating the heat transfer surface area, the problem is reduced to calculating the average heat transfer coefficient and the logarithmic mean temperature difference. The length of the heat exchange device is calculated using the formula $L = F/(\pi nd)$, where n is number of inner tubes and d is their hydraulic diameter.

The temperature distributions along the heat exchange surface are expressed by the relations:

— Parallel flow heat exchanger:

$$T_1(x) = T_1' - \Delta T' \frac{1 - \exp[-\bar{k}mF(x)]}{1 + (G_1 c_{p1})/(G_2 c_{p2})};$$

$$T_2(x) = T_2' + \Delta T' \frac{1 - \exp[-\bar{k}mF(x)]}{1 + (G_2 c_{p2})/(G_1 c_{p1})};$$

— Counterflow heat exchanger:

$$T_1(x) = T_1' - \Delta T' \frac{1 - \exp[-\bar{k}mF(x)]}{1 - (G_1 c_{p1})/(G_2 c_{p2})};$$

$$T_2(x) = T_2'' + \Delta T' \frac{1 - \exp[-\bar{k}mF(x)]}{1 - (G_2 c_{p2})/(G_1 c_{p1})}.$$

Here, $F(x)$ is the dependence of the heat exchange surface area on the length measured along the path of the hot coolant. In the case of a cylindrical surface, the heat transfer

area is expressed in terms of the length $F(x) = \Pi x$, where Π is the wetted perimeter heat exchange surfaces.

For the case of thin cylindrical walls, the relations for surface temperatures have the form

$$T_{w1} = \frac{\left(\frac{\alpha_1 F_1}{\alpha_2 F_2} + \frac{\alpha_1 F_1 \delta_w}{\lambda_w F_a}\right) T_1 + T_2}{1 + \frac{\alpha_1 F_1}{\alpha_2 F_2} + \frac{\alpha_1 F_1 \delta_w}{\lambda_w F_a}};$$

$$T_{w2} = \frac{\left(\frac{\alpha_2 F_2}{\alpha_1 F_1} + \frac{\alpha_2 F_2 \delta_w}{\lambda_w F_a}\right) T_2 + T_1}{1 + \frac{\alpha_2 F_2}{\alpha_1 F_1} + \frac{\alpha_2 F_2 \delta_w}{\lambda_w F_a}}.$$

Here, $F_a = (F_1 + F_2)/2$, F_1 is the heat exchange area from coolant 1 side, F_2 is the heat transfer area from coolant 2 side, δ_w is the thickness wall, λ_w is the thermal conductivity of the wall, and α is the heat transfer coefficient. The relations are implicit and require an iterative solution, since the heat transfer coefficient depend on the temperature.

For a thin single-layer wall, the average heat transfer coefficient is calculated as follows

$$\bar{k} = \left(\frac{1}{\bar{\alpha}_1} + \frac{\delta_w}{\lambda_w} + \frac{1}{\bar{\alpha}_2}\right)^{-1},$$

where $\bar{\alpha}_1$ is average heat transfer coefficient to the cold coolant and $\bar{\alpha}_2$ is average heat transfer coefficient to the hot coolant.

The Nusselt number depends on the flow regime (laminar or turbulent) and the heat transfer regime (heating or cooling). The average heat transfer coefficient is expressed in terms of the Nusselt number averaged over the length $Nu = \bar{\alpha} d_g / \lambda$, where $d_g = 4F_g / \Pi$ is the effective hydraulic diameter, F_g is the flow area channel, Π is the wetted perimeter, and λ is the liquid thermal conductivity. For the flow in a pipe or for the longitudinal flow around bundles of pipes, the Nusselt number is calculated using a semi-empirical dependence of the form

$$Nu = Nu(Re, Pr, Pr_w, L/d_g),$$

where Re is the Reynolds number, Pr is the Prandtl number, and Pr_w is the Prandtl number calculated at the wall temperature. The similarity numbers are calculated from the average coolant temperature. The Reynolds number is defined as $Re = \rho v s. d_g / \mu$, where v is the characteristic flow velocity, ρ is the density, and μ is the dynamic viscosity.

4. Method for Variable Viscosity

In the case of a strong dependence of viscosity on temperature, the heat exchanger is divided into elementary sections along the length. At each section, an assumption is presented about a negligible change in the viscosity. The local Nusselt numbers in the laminar and turbulent flow regimes are found using semi-empirical relations. The transition between different criterion relationships corresponding to laminar, transitional, and turbulent flow regimes is realized depending on the Reynolds number.

With a weak dependence of the viscosity of the coolant on temperature, the average Reynolds number is found from the average temperature of the coolant. Such an assumption does not introduce significant errors into the calculation, since it practically does not affect the flow regime. In the case of a strong dependence of viscosity on temperature, as the coolant heats up, the flow regime changes from laminar to developed turbulent. In this case, the local heat transfer coefficient $\alpha(x)$ is calculated, and the relations for the local Nusselt number $Nu_x = \alpha(x) d_g / \lambda$ calculated from local similarity numbers are used

$$Nu_x = Nu(Re_x, Pr_x, Pr_w, x/d_g).$$

The average value of the heat transfer coefficient is found using the formula

$$\bar{\alpha} = \frac{1}{L} \int_0^L \alpha(x) dx.$$

To calculate the local Nusselt number in the laminar flow regime in a pipe (for $Re < 2 \times 10^3$), the following relation is used [25]:

$$Nu_x = 4.36 \left(1 + 0.032 \frac{d}{x} Re_x Pr_x^{5/6} \right)^{2/5} \left(\frac{Pr_x}{Pr_{x,w}} \right).$$

This relation is valid for $0.7 < Pr < 10^3$. The expression for calculating the local Nusselt number for the turbulent flow in a pipe (for $Re > 10^4$) with an additional correction for the change in the Prandtl number has the form

$$Nu_x = 0.022 Re_x^{0.8} Pr_x^{0.43} \left(\frac{Pr_x}{Pr_{x,w}} \right)^{0.25} \epsilon_l,$$

where

$$\epsilon_l = \begin{cases} 1 & \text{if } x/d \geq 15, \\ \frac{1.38}{(x/d)^{0.12}} & \text{if } x/d < 15. \end{cases}$$

In the transient flow regime, linear interpolation is used. For an annular channel in a turbulent flow regime, the ratio is used as for the flow in a pipe but with its own equivalent hydraulic diameter.

The heat balance equation for an elementary section in the direction of movement of the hot coolant is written in the following form

$$\begin{aligned} \frac{dQ_1}{dx} &= G_1 c_{p1}(T_1) \frac{dT_1}{dx}, & \frac{dQ_1}{dx} &\leq 0; \\ \frac{dQ_2}{dx} &= \pm G_2 c_{p2}(T_2) \frac{dT_2}{dx}, & \frac{dQ_2}{dx} &\geq 0; \\ \frac{dQ_1}{dx} + \frac{dQ_2}{dx} &= 0. \end{aligned} \tag{5}$$

Here, dQ_1 is the loss of the heat quantity by the hot coolant, dQ_2 is the acquired quantity of heat by the cold coolant, G is the mass flow rate of the coolant, c_p is the heat capacity, and dT is the temperature change. The plus sign corresponds to the direct-flow circuit and the minus sign corresponds to the counterflow circuit. The heat transfer equation for an elementary section adopts the form

$$\begin{aligned} \frac{dQ_1}{dx} &= k(T_1, T_2)(T_2 - T_1) \frac{dF}{dx}, & \frac{dQ_1}{dx} &\leq 0; \\ \frac{dQ_2}{dx} &= k(T_1, T_2)(T_1 - T_2) \frac{dF}{dx}, & \frac{dQ_2}{dx} &\geq 0. \end{aligned} \tag{6}$$

Here, k is the local heat transfer coefficient and dF/dx is the change in the heat exchange area, which remains constant for a heat exchanger of straight pipes.

Equations (5) and (6) imply a closed system of equations for coolant temperatures

$$\begin{aligned} \frac{dT_1}{dx} &= \frac{k(T_1, T_2)}{G_1 c_{p1}(T_1)} (T_2 - T_1) \frac{dF}{dx}; \\ \frac{dT_2}{dx} &= \pm \frac{k(T_1, T_2)}{G_2 c_{p2}(T_2)} (T_1 - T_2) \frac{dF}{dx}. \end{aligned} \tag{7}$$

Since $dF/dx = \text{const}$ is known, the system of Equation (7) is a system of ordinary differential equations with a non-linear right-hand side. In the case of a direct-flow scheme (plus sign), the Cauchy problem is posed for the system (7), and, for a counterflow scheme (minus sign), a boundary value problem is solved. In this case, the integration is carried out up to the length L , which is not known in advance.

The system of Equation (7) is solved by the finite difference method on the interval $x \in [0, L]$, which causes it to be possible to apply the developed approach for calculating both the direct-flow and counter-flow heat exchangers. To stabilize the iterative process during the linearization of the system, the under-relaxation method is used. The length of the integration interval L is not known in advance. Newton's method is used to determine it.

5. CFD Simulation

The results of the thermal calculations are compared with the data obtained using the CFD methods. Oil is considered a Newtonian fluid with a constant density. The calculations are carried out using the numerical solution of the RANS equations for a viscous incompressible fluid, closed using a turbulence model that takes into account the laminar–turbulent transition.

The numerical simulation of fluid flow and heat transfer includes the numerical solution of continuity, momentum, and energy transport equations in the computational domain. The flow is described in the Cartesian coordinates. The governing equations for steady state flow have the form:

— Continuity equation:

$$\frac{\partial v_j}{\partial x_j} = 0; \quad (8)$$

— Momentum equation:

$$v_j \frac{\partial v_i}{\partial x_j} = -\frac{1}{\rho} \frac{\partial p}{\partial x_i} + \frac{\partial}{\partial x_i} \left[(v + v_t) \frac{\partial v_i}{\partial x_j} \right]; \quad (9)$$

— Energy equation:

$$v_j \frac{\partial T}{\partial x_j} = \frac{\partial}{\partial x_i} \left[\left(\frac{\nu}{\text{Pr}} + \frac{\nu_t}{\text{Pr}_t} \right) \frac{\partial T}{\partial x_j} \right]. \quad (10)$$

Here, ρ is the density and v_i is the velocity component in the x_i coordinate direction. p is the pressure, T is the temperature, ν is the kinematic viscosity, and Pr is the Prandtl number. Subscript t corresponds to the turbulent flow quantities. For a simulation of the turbulent flows, the linear model employs a Boussinesq stress–strain relation. The eddy viscosity is found from the solution of the transport equations of the turbulence model. Water and oil are Newtonian incompressible fluids. It is assumed for simplicity that water and oil satisfy the equation of the state of ideal gas with their densities.

The turbulence models that are usually used in the CFD simulations of internal and external flows do not take into account the laminar–turbulent transition. In some turbulence models, a transition point is predicted before the calculations based on some additional considerations. In the analysis of the CFD results, a flow transition from the laminar regime to the turbulent is defined using a distribution of the skin friction coefficient. However, this way is not accurate and could not be applied to a wide range of practical applications. There are a limited number of turbulence models taking into account the laminar–turbulent transition.

The SST turbulence model is designed to efficiently combine the reliable k – ω model in the near-wall region and k – ϵ model in free flow [26,27]. To switch between models, a

special function is used that removes a unit value in the near-wall region (the standard $k-\omega$ model is used) and a zero value away from the wall (the $k-\epsilon$ model is used).

The model that takes into account the laminar–turbulent transition (Local-Correlation Transition Model, γ - $Re_{\theta t}$ transition model) is based on a combination of the equations of the SST turbulence model with two additional transport equations for the intermittency parameter γ and the critical Reynolds number $Re_{\theta t}$ constructed from the momentum loss thickness [28,29].

The turbulence model, proposed in [28], includes solutions for two extra transport equations. One equation is written for the transition onset momentum thickness Reynolds number, $Re_{\theta t}$ (it is included into the correlation between the location of the transition onset and transition location), and the other equations is derived for the intermittency, γ (measure of the flow regime). The transport equations for the momentum thickness Reynolds number and intermittency have the form:

— Equation for momentum thickness Reynolds number:

$$v_j \frac{\partial Re_{\theta t}}{\partial x_j} = P_{\theta t} + \frac{\partial}{\partial x_j} \left[\sigma_{\theta t} (v + v_t) \frac{\partial Re_{\theta t}}{\partial x_j} \right]; \quad (11)$$

— Equation for intermittency:

$$v_j \frac{\partial \gamma}{\partial x_j} = P_\gamma - E_\gamma + \frac{\partial}{\partial x_j} \left[\left(v + \frac{v_t}{\sigma_\gamma} \right) \frac{\partial \gamma}{\partial x_j} \right]. \quad (12)$$

Here, $P_{\theta t}$ is the production term of the momentum thickness Reynolds number, P_γ and E_γ are production and dissipation terms of the intermittency, $\sigma_{\theta t}$ and σ_γ are constants of the model.

The mass flow rate is specified in the inlet section of the tube, and the free outflow boundary conditions are applied to the outlet section. The external tube is considered as perfectly insulated with the specification of the adiabatic boundary conditions on the solid wall.

To simplify the model, the equation for $Re_{\theta t}$ is not considered, and the equation for the intermittency parameter assumes that the convective terms are small [30]. This approach leads to algebraic relations for finding the intermittency parameter. The γ - $Re_{\theta t}$ model used in the calculations was developed to solve problems in the external aerodynamics. Subsequently, the model was used to simulate a wide range of flows. In particular, [31] compared different turbulence models ($k-\epsilon$, $k-\omega$, $k-\omega$ SST, v^2-f , γ - Re_θ) applied to the flow in the channel.

To discretize the governing Equations (8)–(12), the finite volume method on unstructured meshes is used [32]. The computational procedure employs the time marching algorithm. Time integration is carried out by the third order Runge–Kutta method. The inviscid fluxes are discretized using the MUSCL (Monotonic Upstream Schemes for Conservation Laws) scheme, and the viscous fluxes are discretized using a centred scheme of the second order. The MUSCL scheme causes it to be possible to increase the order of approximation in the spatial variables without losing the monotonicity of the solution, satisfies the TVD (Total Variation Diminishing) condition, and is a combination of the centred finite differences of the second order and a dissipative term, which are switched between using a flux limiter built on the basis of characteristic variables. The geometric multigrid method [33] is used to solve the system of difference equations.

The energy balance equation for the solid domain is written as

$$\rho c \frac{\partial T}{\partial t} = \frac{\partial}{\partial x_i} \left(\lambda \frac{\partial T}{\partial x_j} \right), \quad (13)$$

where ρ is the density, c is the specific heat capacity, and λ is the thermal conductivity. The internal heat sources in Equation (13) are neglected.

To perform mesh sensitivity analysis, the boundary layer velocity profiles computed with various meshes are assessed. The comparison of the velocity profiles is presented in Figure 3. The Reinhard's law covering the boundary layer region (line 1), linear (line 2), and logarithmic (line 3) velocity profiles are also presented. The symbols \square , \bullet , and \circ correspond to meshes with 12 (mesh 1), 24 (mesh 2), and 48 (mesh 3) nodes in the normal direction (the number of nodes in a stream-wise directions is the same for the three meshes). The results obtained show that the velocity profiles computed with meshes 2 and 3 are similar and the maximum discrepancy between them is not larger than 3%. Mesh 2 is used in the CFD simulations.

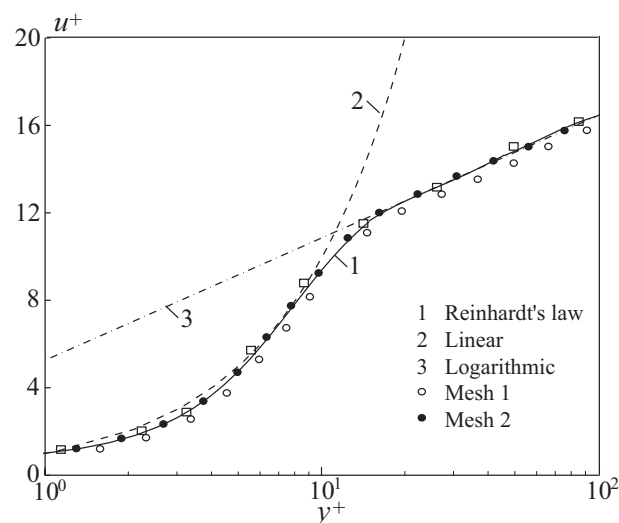


Figure 3. Velocity profiles in the boundary layer.

The calculations use a mesh consisting of 19,461 cells, of which 500×24 cells are placed in the area filled with oil, 500×5 cells are placed in the steel area, and 500×13 cells are placed in an area filled with water (Figure 4). The cells are thickened near the pipe walls in such a way that $y^+ < 2$, where y^+ is the dimensionless near-wall coordinate. To achieve this, 15 mesh nodes are placed in the near-wall layer; the distance between varies according to the law of geometric progression.

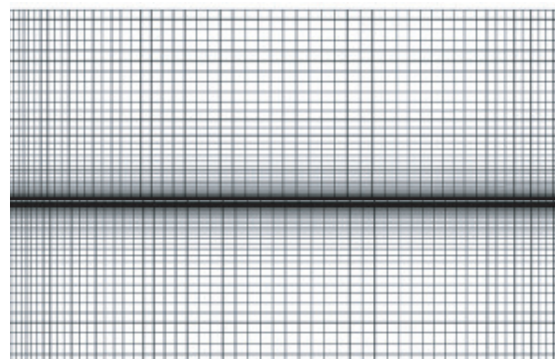


Figure 4. Mesh used in CFD calculations.

To control the convergence of the iterative process, the discrepancy level of the unknown physical quantities and satisfying of the mass balance equation are verified. The calculations are terminated when the level of discrepancy of all the physical quantities decreases by three orders of magnitude, and the mismatch of the mass flow rates at the input and output boundaries of the computational domain becomes less than 10^{-3} kg/s.

6. Results and Discussion

The forward flow scheme was chosen as a model. The developed approach does not impose restrictions on the scheme of the heat exchanger used. For the ordinary differential equations with constant or variable viscosity, the Cauchy problem is not solved (which is obtained only with the parallel flow scheme) but the boundary value problem (in the case of the parallel flow scheme, the boundary conditions are set at one end, and, in the counterflow scheme, the boundary conditions are specified at different ends of the pipes).

Figure 5 shows the diagram of a parallel flow heat exchanger (the dimensions are provided in millimetres). The index h corresponds to a hot medium (water) and the index c corresponds to a cold medium (oil). The indices i and o refer to the inlet and outlet sections.

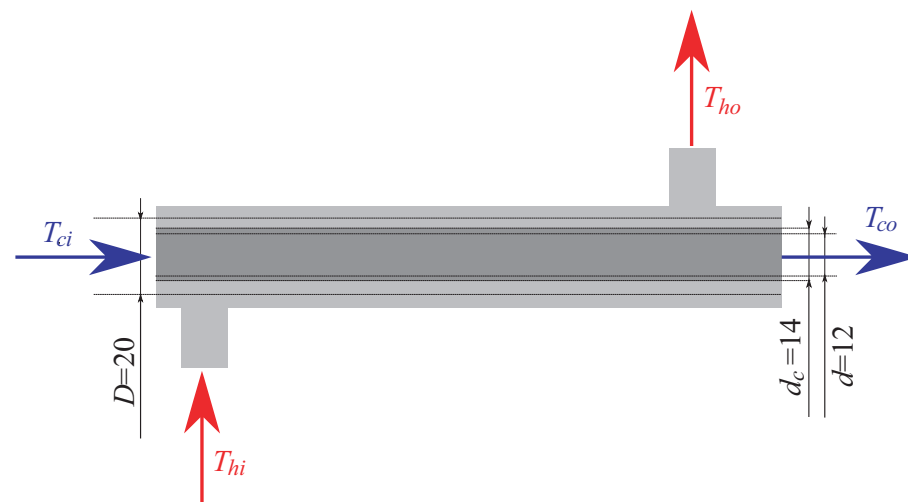


Figure 5. Scheme of parallel flow heat exchanger (dimensions are provided in millimetres).

To calculate the effective length of the heat exchanger and the temperature of the hot heat carrier at the outlet, the parameters provided in Table 1 are specified (inlet and outlet temperatures of the cold heat carrier, inlet temperature of the hot and outer tubes, and the physical properties of the tube material).

Table 1. Input parameters for thermal calculations.

Quantity	Units	Symbol	Number
Number of tubes		n	1
Wall thickness	mm	δ_w	1
Inner diameter	mm	d	12
Outer diameter	mm	d_c	14
Inner diameter of shroud	mm	D	20
Inlet temperature of hot stream	K	T_{hi}	423
Mass flow rate of hot fluid	kg/s	G_h	0.6386
Speed of hot fluid	m/s	v_h	4
Inlet temperature of cold fluid	K	T_{ci}	303
Outlet temperature of cold fluid	K	T_{co}	328
Mass flow rate of cold fluid	kg/s	G_c	0.3814
Speed of cold fluid	m/s	v_c	4

To calculate the effective length of the heat exchanger and the temperature of the hot coolant at the outlet, the following parameters are set: $T_{ci} = 303$ K and $T_{co} = 328$ K (inlet and outlet temperatures of the cold coolant), $T_{hi} = 423$ K (hot coolant inlet temperature), $v_c = 4$ m/s and $v_h = 4$ m/s (cold and hot coolant velocities), $G_c = 0.3814$ kg/s and $G_h = 0.6386$ kg/s (mass flow rates of hot and cold coolant), geometric characteristics (tube wall thickness $\delta_w = 1$ mm, inner and outer diameters of tubes $d = 12$ mm and $d_c = 14$ mm, casing inner diameter $D = 20$ mm), and the physical properties of the tube material. The

transitions between different semi-empirical Equations (laminar, transient, and turbulent) are implemented by a jump based on the Reynolds number calculated from the average mass velocity.

The heat balance equations are used to determine the hot outlet temperature and the corresponding effective length of the heat exchanger. Solving the heat balance equations using the finite difference method, the distributions of the mass-average coolant temperatures provided in Table 2 are obtained. Solving the heat balance equations by the finite difference method, the length of the heat exchanger is $L = 5.28$ m in the case of the constant viscosity and the length of the heat exchanger is $L = 4.26$ in the case of the variable viscosity. In both cases, the temperature of the hot coolant at the outlet reaches 416 K.

Table 2. Results of calculations.

Model	With Constant Viscosity	With Variable Viscosity
Length, m	5.2788	4.2643
Outlet temperature of hot fluid, K	415.9922	415.9921

The results obtained are compared with the CFD data. Figure 6 shows the distributions of the mass-average temperature of oil (cold coolant) along the length of the heat exchanger, obtained using the finite difference method and based on the numerical simulation. The mass-average oil temperature increases along the length due to heating from a heat source (hot coolant). The results of the theoretical and numerical calculations are in good agreement with each other.

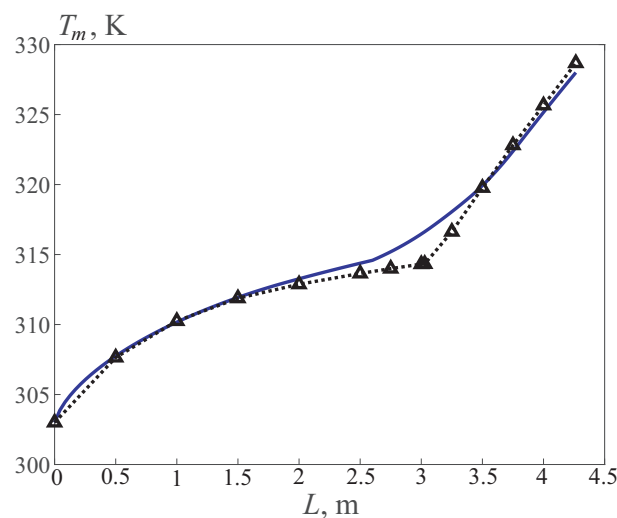


Figure 6. Distributions of the mass average temperature of oil along the length. The solid line corresponds to the results obtained on the basis of the theoretical approach, and the dotted line with triangular marks corresponds to the results of numerical calculations.

The distributions of the mass-average temperature of water (hot coolant) along the length, obtained on the basis of theoretical and numerical calculations, are shown in Figure 7. Compared to the results shown in Figure 6, the mass-average water temperature decreases along the length due to the heat transfer from it to the cold coolant. It should also be noted that there is a good agreement between the results of the calculations obtained on the basis of different approaches.

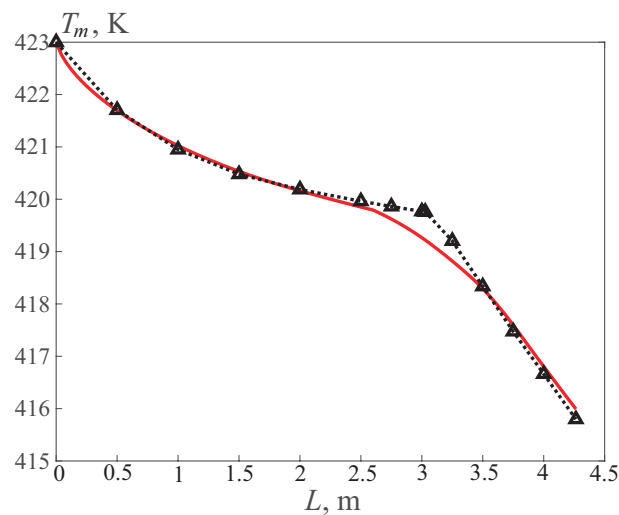


Figure 7. Mass-average water temperature distributions along the length. The solid line corresponds to the results obtained on the basis of the theoretical approach, and the dotted line with triangular marks corresponds to the results of numerical calculations.

From the results shown in Figures 6 and 7, one can notice the characteristic changes in the curvature of the lines at a distance of about 2.5 m from the inlet section, where, in both cases, there are sharp changes in the temperature gradients with the corresponding signs. This transition occurs at the distance where the laminar flow regime becomes turbulent. Figure 8 shows graphs of the change in the Reynolds number of coolants along the length, obtained in the calculation based on the model with the variable viscosity. For water, the Reynolds number practically does not change along the length at a constant value of viscosity and a slight change in the water temperature. The reverse picture is observed for a cold coolant (oil). The Reynolds number increases significantly along the length, which is associated with a sharp decrease in the viscosity of oil at its practically unchanged density. The figure also shows a transitional section at a distance from about 1.85 to 3.8 m, where the transition from the laminar to turbulent flow occurs.

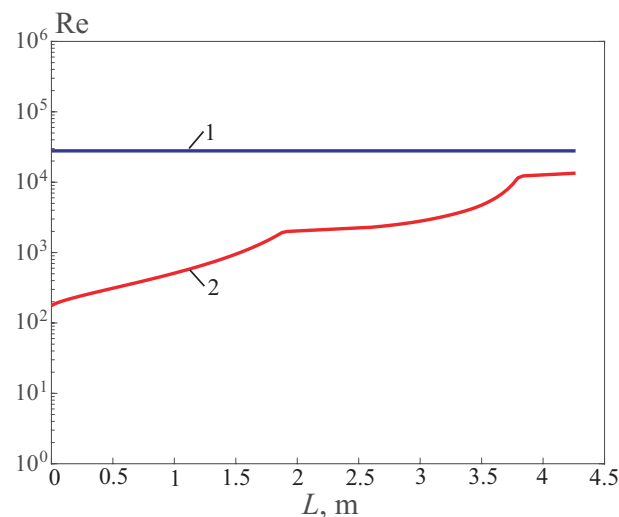


Figure 8. Distributions of Reynolds numbers obtained in a theoretical calculation. Line 1 corresponds to water, and line 2 corresponds to oil.

Figure 9 shows a graph of the change in the Reynolds number of oil (cold coolant) along the length of the heat exchanger at variable oil viscosity (line 1). The values of the Reynolds number sharply increase along the longitudinal coordinate, which is explained by a decrease in the viscosity of oil due to its heating. The figure also shows a graph of the

behaviour of the Reynolds number of oil at an average coolant temperature (line 2). At a constant viscosity, the Reynolds number of the cold coolant is also constant along the length and cannot adequately characterize the heat transfer in a given heat exchanger. The first break corresponds to switching formulas at $Re \sim 2 \times 10^3$ (transition from laminar to transitional flow), and the second break corresponds to switching formulas at $Re \sim 10^4$ (transition from transitional flow regime to turbulent). The work uses three sections and three different sets of formulas (laminar, transitional, and turbulent).

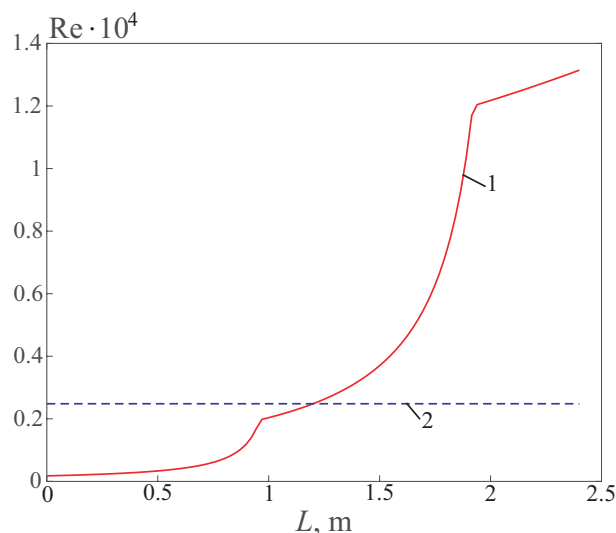


Figure 9. Distributions of oil Reynolds numbers along length. Line 1 corresponds to the numerical calculation at variable viscosity, and line 2 corresponds to the theoretical calculation.

The distribution of the axial velocity of the coolant (oil) in various cross sections of the pipeline is shown in Figure 10. In the cross section, the oil velocity varies from the maximum value on the axis of the pipeline to zero on its surface. The increase in the axial velocity at the outlet is explained by the decrease in the oil viscosity due to its heating as it approaches the outlet section. In this case, a turbulent flow regime occurs for oil.

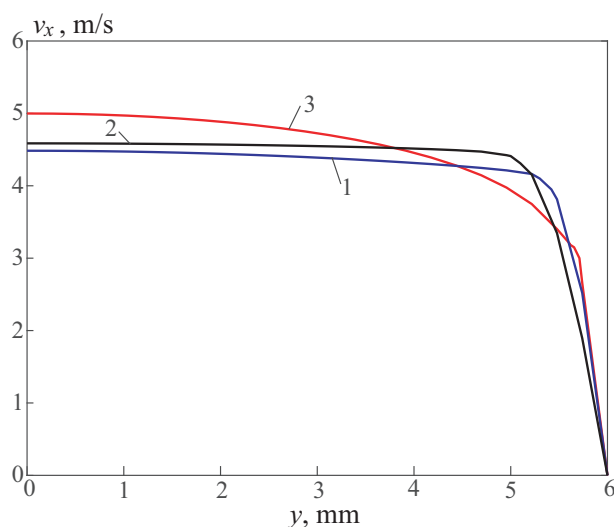


Figure 10. Radial distributions of oil axial velocity in different pipeline cross sections at $x = 0.5$ m (line 1), $x = 1.5$ m (line 2), and in the exit section (line 3).

Fluid enters the tube with a uniform velocity. When the fluid contacts the surface, viscous effects become important, and a boundary layer develops with an increasing axial coordinate. This development occurs at the expense of a shrinking inviscid flow region and concludes with the boundary layer merger at the centreline (hydrodynamic entry region).

Following this merger, the viscous effects extend over the entire cross section, and the velocity profile no longer changes with the increasing axial coordinate (fully developed flow). The fully developed velocity profile is parabolic for the laminar flow in a circular tube. For the turbulent flow, the profile is flatter due to turbulent mixing in the radial direction. If a fluid enters the tube at a uniform temperature that is less than the surface temperature, convection heat transfer occurs, and a thermal boundary layer begins to develop. Moreover, if the tube surface condition is fixed by imposing either a uniform temperature or a uniform heat flux, a thermally fully developed condition is eventually reached. The shape of the fully developed temperature profile differs according to whether a uniform surface temperature or heat flux is maintained. For both surface conditions, however, the amount by which the fluid temperatures exceed the entrance temperature increases with the increasing axial coordinate.

The distribution of the axial velocity of water in the outlet section of the pipeline is shown in Figure 11. The water velocity changes from zero on the wall to a maximum value on the channel axis. The flow of the water in this case is turbulent. The velocity profile has a character typical of the turbulent flow in a round pipe, being more filled near the axis and having large velocity gradients near the wall compared to the laminar flow.

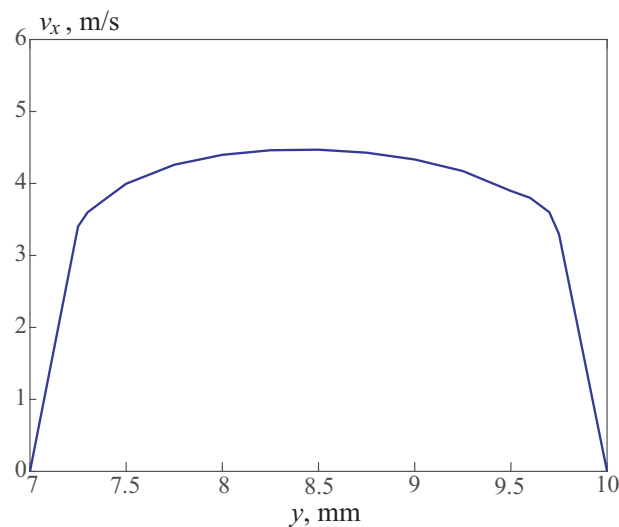


Figure 11. Radial distribution of the axial water velocity in the outlet section.

The temperature distribution along the wall of the pipe through which the cold coolant flows is shown in Figure 12. The temperature remains almost constant up to the cross section $x = 3.2$ m, after which a sharp increase in the temperature is observed. This behaviour is associated with the transition from the laminar flow regime to the turbulent one. At the inlet, the oil is cold and the wall on the oil side cools down strongly, then it warms up (heat transfer by thermal conductivity predominates), a laminar–turbulent transition occurs, the heat transfer increases significantly, and the wall temperature decreases.

On the graphs of the temperature distribution along the pipe, there is a steepening of the profile at the beginning of the transition zone (2.5–3 m), i.e., an increase in the heat exchange intensity. For example, if we consider a graph showing the distribution of the coefficient of friction along the length of the pipe, then, in the transition region, there is a dip in the coefficient of friction near the transition region.

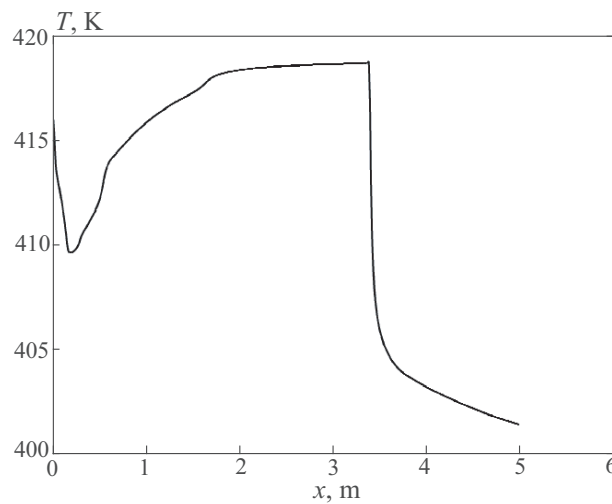


Figure 12. Temperature distributions along the pipe wall from the oil side.

The distribution of the cross section-averaged oil pressure is shown in Figure 13. In this case, the pressure drop along the entire length of the pipe is 51,613.89 Pa.

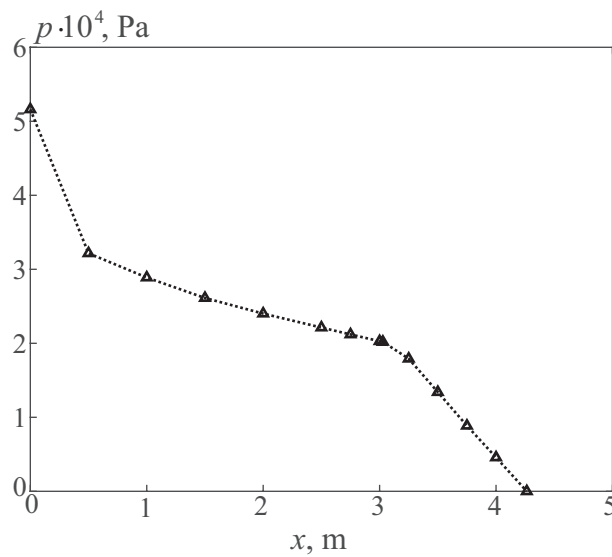


Figure 13. Distribution of cross-section averaged oil pressure.

The change in the friction loss coefficient along the length of the pipe is shown in Figure 14. The coefficient of the friction is calculated locally on a certain interval using the relation $\Delta p / \Delta x / (\rho v^2)$, where Δx is the distance between two points, in which the pressure is measured, and Δp is pressure difference at these points.

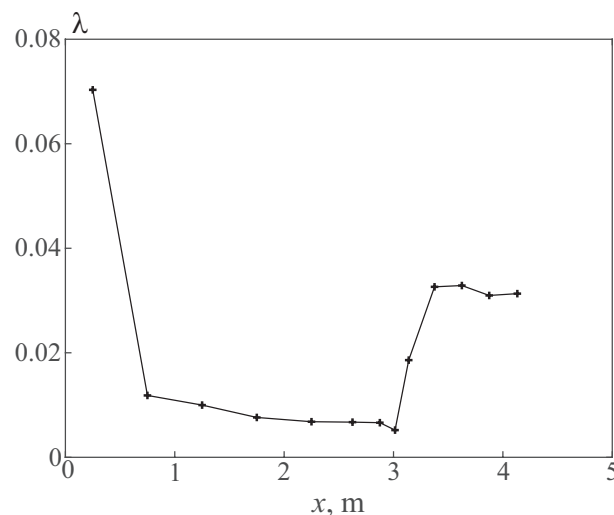


Figure 14. Distribution of the coefficient of friction along the length of the pipe.

7. Conclusions

Thermal and numerical calculations were carried out to determine the length of the heat exchanger and the temperature of the cold coolant in the outlet section in the case of constant and variable oil viscosity. The length of the heat exchanger was also determined using CFD calculations in a turbulence model that takes into account the laminar–turbulent transition. With a variable viscosity of oil, a transition from a laminar regime to a turbulent one is manifested, while, in the theoretical calculation method for a constant viscosity, this effect is not taken into account. The results obtained show that the model with constant viscosity leads to an underestimation of the length of the heat exchanger by about 20% compared to the calculations that take into account the dependence of the oil viscosity on temperature.

Author Contributions: Conceptualization, methodology and software, validation, A.K.; formal analysis, investigation, D.K.; writing—original draft preparation, writing—review and editing, K.V.; visualization, D.K.; supervision, N.J.; project administration, N.J. All authors have read and agreed to the published version of the manuscript.

Funding: This research received no external funding.

Institutional Review Board Statement: Not applicable.

Informed Consent Statement: Not applicable.

Data Availability Statement: Not applicable.

Conflicts of Interest: The author declares no conflict of interest.

References

1. Fukai, J.; Mitani, H.; Nakaso, K. Convection heat transfer in a shell and tube heat exchanger using sheet fins for effective utilization of energy. *Int. J. Heat Mass Transf.* **2015**, *82*, 581–587.
2. Wang, Y.; Gu, X.; Jin, Z.; Wang, K. Characteristics of heat transfer for tube banks in crossflow and its relation with that in shell-and-tube heat exchangers. *Int. J. Heat Mass Transf.* **2016**, *93*, 584–594. [[CrossRef](#)]
3. Araavind, S.; Athreya, A.S. CFD analysis of shell and tube heat exchanger for pre-heating of biodiesel. *Int. Adv. Res. Sci. Eng.* **2017**, *6*, 687–693.
4. Abda, A.A.; Kareema, M.Q.; Najib, S.Z. Performance analysis of shell and tube heat exchanger: Parametric study. *Case Stud. Therm. Eng.* **2018**, *12*, 563–568. [[CrossRef](#)]
5. Lychakov, V.D.; Egorov, M.Y.; Shcheglov, A.A.; Sivovolov, A.S.; Matyash, A.S.; Balunov, B.F. Heat transfer analysis of assemblies of finned heat exchangers. *Therm. Eng.* **2022**, *3*, 63–72.
6. Darbandi, M.; Abdollahpour, M.-S.; Hasanpour-Matkolaei, M. A new developed semi-full-scale approach to facilitate the CFD simulation of shell and tube heat exchangers. *Chem. Eng. Sci.* **2021**, *245*, 116836. [[CrossRef](#)]
7. Bizhan, K.G.; Mohammad, R.D.; Hossein, P. Prediction of kinematic viscosity of petroleum fractions using artificial neural networks. *Iran. J. Oil Gas Sci. Technol.* **2014**, *3*, 51–65.

8. Boda, M.A.; Bhasagi, P.N.; Sawade, A.S.; Andodgi, R.A. Analysis of kinematic viscosity for liquids by varying temperature. *Int. J. Innov. Res. Sci. Eng. Technol.* **2015**, *4*, 1951–1954.
9. Lee, B.I.; Kesler, M.G. A generalized thermodynamic correlation based on three-parameter corresponding states. *AIChE J.* **1975**, *21*, 510–527. [[CrossRef](#)]
10. Aralov, O.V.; Buyanov, I.V.; Savanin, A.S.; Iordansky, E.I. Research of methods for oil kinematic viscosity calculation in the oil-trunk pipeline. *Sci. Technol. Oil Oil Prod. Pipeline Transp.* **2017**, *7*, 97–105. [[CrossRef](#)]
11. Yogesh, S.S.; Selvaraj, A.S.; Ravi, D.K.; Rajagopal, T.K.R. Heat transfer and pressure drop characteristics of inclined elliptical fin tube heat exchanger of varying ellipticity ratio using CFD code. *Int. J. Heat Mass Transfer* **2018**, *119*, 26–39. [[CrossRef](#)]
12. Chen, K.; Mohammed, H.I.; Mahdi, J.M.; Rahbari, A.; Cairns, A.; Talebizadehsardari, P. Effects of non-uniform fin arrangement and size on the thermal response of a vertical latent heat triple-tube heat exchanger. *J. Energy Storage* **2022**, *45*, 103723. [[CrossRef](#)]
13. Osley, W.G.; Droegemueller, P.; Ellerby, P. CFD investigation of heat transfer and flow patterns in tube side laminar flow and the potential for enhancement. *Chem. Eng. Trans.* **2013**, *35*, 997–1002.
14. Karar, O.; Emani, S.; Gounder, S.M.; Myo Thant, M.M.; Mukhtar, H.; Sharifpur, M.; Sadeghzadeh, M. Experimental and numerical investigation on convective heat transfer in actively heated bundle-pipe. *Eng. Appl. Comput. Fluid Mech.* **2021**, *15*, 848–864. [[CrossRef](#)]
15. Rana, S.; Zunaid, M.; Kumar, R. CFD approach for the enhancement of thermal energy storage in phase change material charged heat exchanger. *Case Stud. Therm. Eng.* **2022**, *33*, 101921. [[CrossRef](#)]
16. Allouche, Y.; Varga, S.; Bouden, C.; Oliveira, A.C. Validation of a CFD model for the simulation of heat transfer in a tubes-in-tank PCM storage unit. *Renew. Energy* **2016**, *89*, 371–379. [[CrossRef](#)]
17. Balaji, D.; Prakash, L.S.S. CFD analysis of a pressure drop in a staggered tube bundle for a turbulent cross flow. *Int. Adv. Res. J. Sci. Eng. Technol.* **2016**, *3*, 35–40.
18. Czarnota, T.; Wagner, C. Turbulent convection and thermal radiation in a cuboidal Rayleigh–Benard cell with conductive plates. *Int. J. Heat Fluid Flow* **2016**, *57*, 150–172. [[CrossRef](#)]
19. Mohanan, A.K.; Prasad, B.V.; Vengadesan, S. Flow and heat transfer characteristics of a cross-flow heat exchanger with elliptical tubes. *Heat Transf. Eng.* **2020**, *42*, 1846–1860. [[CrossRef](#)]
20. Fathi, S.; Yazdi, M.E.; Adamian, A. Numerical investigation of heat transfer enhancement in heat sinks using multiple rows vortex generators. *J. Theor. Appl. Mech.* **2020**, *58*, 97–108. [[CrossRef](#)]
21. Lindqvist, K.; Skaugen, G.; Meyer, O.H.H. Plate fin-and-tube heat exchanger computational fluid dynamics model. *Appl. Therm. Eng.* **2021**, *189*, 116669. [[CrossRef](#)]
22. Ojaniemi, U.; Pättikangas, T.; Jäsberg, A.; Puhakka, E.; Koponen, A. Computational fluid dynamics simulation of fouling of plate heat exchanger by phosphate calcium. *Heat Transf. Eng.* **2022**, *43*, 1396–1405. [[CrossRef](#)]
23. Arsenyeva, O.; Matsegora, O.; Kapustenko, P.; Yuzbashyan, A.; Klemes, I.J. The water fouling development in plate heat exchangers with plates of different corrugations geometry. *Therm. Sci. Eng. Prog.* **2022**, *32*, 101310. [[CrossRef](#)]
24. Tugunov, P.I.; Novoselov, V.F.; Korshak, A.A.; Shammazov, A.M. *Standard Calculations for the Design and Operation of Tank Farms and Oil Pipelines*; Design Polygraph Service: Moscow, Russia, 2002.
25. Sachenko, V.P.; Osipova, V.A.; Sukomel, A.S. *Heat Transfer*; Energy: Moscow, Russia, 1965.
26. Menter, F.R. Two-equation eddy-viscosity turbulence models for engineering applications. *AIAA J.* **1994**, *32*, 1598–1605. [[CrossRef](#)]
27. Menter, F.; Esch, T.; Kubacki, S. *Transition Modelling Based on Local Variables. Engineering Turbulence Modelling and Experiments*; Elsevier: Amsterdam, The Netherlands, 2002; pp. 555–564.
28. Langtry, R.B.; Menter, F.R. Correlation-based transition modeling for unstructured parallelized computational fluid dynamics codes. *AIAA J.* **2009**, *47*, 2894–2906. [[CrossRef](#)]
29. Coder, J.G.; Maughmer, M.D. Computational fluid dynamics compatible transition modeling using an amplification factor transport equation. *AIAA J.* **2014**, *52*, 2506–2512. [[CrossRef](#)]
30. Menter, F.R.; Smirnov, P.E.; Liu, T.; Avancha, R. A one-equation local correlation-based transition model. *Flow Turbul. Combust.* **2015**, *95*, 583–619. [[CrossRef](#)]
31. Gorji, S.; Seddighi, M.; Ariyaratne, C.; Vardy, A.E.; O’Donoghue, T.; Pokrajac, D.; He, S. A comparative study of turbulence models in a transient channel flow. *Comput. Fluids* **2014**, *83*, 111–123. [[CrossRef](#)]
32. Volkov, K. *Numerical Analysis of Navier–Stokes Equations on Unstructured Meshes*; Nova Science: Hauppauge, NY, USA, 2016; pp. 365–442.
33. Volkov, K. *Multigrid and Preconditioning Techniques in CFD Applications*; Springer International Publishing: Berlin/Heidelberg, Germany, 2018; pp. 83–149.

Disclaimer/Publisher’s Note: The statements, opinions and data contained in all publications are solely those of the individual author(s) and contributor(s) and not of MDPI and/or the editor(s). MDPI and/or the editor(s) disclaim responsibility for any injury to people or property resulting from any ideas, methods, instructions or products referred to in the content.